

Adhesion properties of printable polymer-modified concrete for rock tunnel linings

Yaxin Tao^{1,2}, Gieljan Vantghem¹, Karel Lesage¹, Yong Yuan³, Wouter De Corte^{1,2}, Kim
Van Tittelboom^{1,*}, Geert De Schutter^{1,2,*}

¹*Magnel-Vandepitte Laboratory for Structural Engineering and Building Materials, Ghent University, Ghent, Belgium*

²*Belgium-China Joint Laboratory for Industrialized Construction (Ghent), Ghent University, Ghent, Belgium*

³*State Key Laboratory of Disaster Reduction in Civil Engineering, Tongji University, Shanghai, China*

* Corresponding Author:

Kim.VanTittelboom@UGent.be (Kim Van Tittelboom)

Geert.DeSchutter@UGent.be (Geert De Schutter)

Abstract

Shotcrete used for rock tunnel linings calls for skilled technicians, which is the key aspect to control the rebound. 3D concrete printing of tunnel linings has the potential to reduce manual labor for construction workers and to eliminate rebound, especially at overhead positions. In this study, the sag resistance and bond properties of printable concrete for overhead applications were explored. Mixtures with the addition of redispersible polymer powders and cellulose ethers were formulated. Roughened concrete slabs were used to replace the tunnel wall rock. A tack test with a loading control mode and a stress growth

test were performed. To verify the results of the tack test and the stress growth test, a 3D concrete printing test, involving upside-down printing against the lower face of a supported concrete slab, was performed afterwards. Also, a pull-off test was performed to measure the bond strength of the printed layers in the hardened stage. The results showed that sag resistance of printable concrete is related to two aspects including the adhesion at the interface and the shear resistance of the fresh material itself. The adhesion and shear resistance properties determined two different failure modes (i.e. adhesion failure and cohesion failure). The results also demonstrated that the tack test results were more consistent with the upside-down printing test results, compared to the stress growth test.

Keywords: Printable concrete; rock tunnel lining; tack test; adhesion; redispersible polymer powder, cellulose ether.

1. Introduction

Shotcrete, also known as sprayed concrete, is a method of applying concrete with a high air pressure onto a vertical or overhead surface, including the dry-mix process and the wet-mix process (1). Due to the advantages of high flexibility, convenience, and no requirement of formwork, shotcrete has been widely used in situations where access is difficult, standard concrete casting is not possible, and rapid setting is required (e.g. structural repairs, soil stabilization, avoidance of water penetration, and slope protection). Nevertheless, the support of rock in mining and tunnel linings is probably the most

important application of shotcrete. In tunnel applications, shotcrete is usually sprayed onto the excavation surface to hold the surrounding rock, enhance stability, and prevent oxidation, deterioration, and softening (2).

Unfortunately, several drawbacks appear during the shotcrete process including a low dimensional accuracy of the sprayed profile, pollutions such as wastewater pollution and dust formation, and a high rebound (3). Compared to a rebound of around 30-40% during the dry-mix process, the wet mix process can achieve a lower rebound of 5-15%. However, the rebound cannot be eliminated because of the presence of the pneumatic component required to project and compact shotcrete. Rebound materials that do not adhere to the excavation surface lead to economic problems (e.g. increased production costs) and alterations in the composition of shotcrete (e.g. paste/aggregate ratio) (4).

Compared to the traditional shotcrete technology, 3D concrete printing (3DCP), also known as digital fabrication of concrete, has the potential to avoid the above-mentioned drawbacks of shotcreting (5, 6). With a precise movement of the printing nozzle, the surface quality of the printed rock tunnel linings is expected to be higher than that of shotcrete. Instead of spraying fast with injected high-pressure air, a steady flow of 3D printed materials avoids rebound and dust pollution. In addition, a faster construction rate can be reached in 3DCP because of higher layer thickness. A schematic view of 3D printing of a rock tunnel lining is shown in Fig. 1.



Fig. 1 Schematic view of 3D printing of a rock tunnel lining.

Different from common 3D printed structures that are printed layer by layer from the ground surface, fresh materials should be placed against the excavated wall rock in 3D printing of a tunnel lining. Therefore, sag resistance is required immediately after extrusion to avoid detaching, especially for the overhead positions where the fresh materials are exposed to the falling risk more than anywhere else. It is therefore essential to evaluate the sag resistance of fresh printable materials, as well as the bond strength after hardening.

Lessons could already be learned from the components of repair mortars. Commercially available repair mortars are usually modified with a redispersible polymer powder (RDP) and a cellulose ether (CE) (7, 8). RDP can be obtained by drying liquid polymer dispersions and can be used as a powder component in dry-mix mortar formulations. When mixed with water, the powder redisperses and forms films in the cement matrix (9). Commonly-used RDP includes elastomeric powders such as styrene-butadiene rubber and thermoplastic powders such as poly (ethylene-vinyl acetate), poly (vinyl acetate-vinyl versatate), poly

(styrene-acrylic ester), and polyacrylic ester (10). CE is another commonly-used polymer in repair materials to obtain some of the required properties such as reducing the absorption of water into the porous substrate and increasing the cement hydration and mechanical strength of the mortar (11). These cellulose derivatives are generated from wood fibers or refined short cotton fibers as the main raw materials, after chemical treatment, and by the reaction with etherifying agents (7). Among the wide variety of existing cellulose ethers, four types are usually used including methylcellulose, hydroxypropylmethyl cellulose, hydroxyethylmethyl cellulose, and hydroxyethyl cellulose (12, 13). It should be noted that the properties of CE depend on both the molecular weight of the polymer and on the degree of etherification. However, such information is not generally provided and considered to be kept confidential by the manufacturers. It has been demonstrated that the average molecular weight of the polymer is linked to its solution viscosity when it is dissolved in water at a set concentration and reference temperature (12).

Although the working mechanism and application of RDP and CE have been widely explored for the application in repair mortars, the effect of these admixtures on the performance of printable concrete for rock tunnel linings has not been studied yet. Therefore, it is essential to explore the effect of RDP and CE aiming at enhancing the sag resistance performance of 3D printable concrete, as well as the bond strength. The adhesive properties of cement-based materials are mostly measured after the final setting and only a few test methods focus on the adhesive properties in the fresh stage. The tack test provides one way for measuring the adhesive properties in the fresh stage. During a tack test, two solid surfaces, between which the fresh material is inserted, are pulled away at a

fixed velocity or loading rate after a certain duration. The force versus separating displacement (or time) is then recorded. The tack test has been widely used to characterize the debonding properties of different types of soft materials such as pressure-sensitive adhesives (14, 15) and smectite muds (16). In addition, this method has also been employed more recently to investigate the adhesive properties of cement paste with the addition of polymers (17), fibers (18), and purified attapulgite clays (19).

In this paper, the effect of admixtures including RDP and CE on the properties of 3D printable concrete for rock tunnel linings was evaluated. The sag resistance in the fresh stage and bond strength in the hardened stage were explored. Firstly, seven mixtures modified with different dosages of RDP and CE were formulated and a tack test with a loading control mode was performed for measuring the adhesive strength of printable concrete in the fresh stage. Secondly, a stress growth test with a constant shear rate was used to measure the shear resistance of fresh printable concrete for a better understanding of the adhesion performance. Thirdly, an upside-down printing test against the lower face of a supported concrete slab was performed for measuring the sag resistance and for comparison with the tack test results and stress growth test results. Finally, a pull-off test was performed to compare the bond strength of printable concrete in the hardened stage. The results showed that the addition of RDP had a slightly negative effect on fresh properties. While the addition of CE enhanced the adhesion at the interface, it resulted in a decrease of the shear resistance of the fresh material for high dosages, resulting in a transition from an adhesive failure (i.e. failure occurring at the interface) to a cohesive failure (i.e. failure occurring in the fresh material). In addition, the tack test results were

more consistent with the upside-down printing test results including the maximum layers and failure mode, compared to that of the stress growth test. Pull-off test results presented that RDP had a positive effect on the bond strength while CE had a negative effect.

2. Experimental program

2.1. Materials

Portland cement (PC, Holcim CEM I 52.5 N, specific gravity 3160 kg/m³, blaine specific area 408 m²/kg) and silica sand (specific gravity 2650 kg/m³, maximum particle size 2 mm, fineness modulus 2.05) were used. Liquid polycarboxylate ether (PCE, BASF MasterGlenium 51, concentration 35%) was used as the superplasticizer. One type of redispersible polymer powder (RDP, VINNAPAS 5010N, main component ethylene-vinyl acetate) and two types of cellulose ethers (CE) including CE1 (SE Tylose MH300P2, main component methyl hydroxyethyl cellulose, viscosity 400-700 mPa·s) and CE2 (SE Tylose MB60000P2, main component hydroxyethylmethyl cellulose, viscosity 28000-34000 mPa·s) were chosen. The viscosity of CE represents the viscosity of a 1.9% CE solution which is measured by a Brookfield viscometer (20 rpm, temperature 20 °C, humidity 20%).

Seven mixtures were formulated including one reference mixture (REF), two RDP-modified mixtures (RDP-0.2% and RDP-0.6%), and four CE-modified mixtures (CE1-0.2%, CE2-0.2%, CE2-0.4%, and CE2-0.6%). The sand to binder ratio was fixed as 1 and

the water to binder ratio was fixed as 0.35 for all mixtures. The dosage of PCE was fixed as 0.1% by mass of binder. The addition levels of RDP were 0.2% and 0.6% by mass of binder respectively for RDP-0.2% and RDP-0.6% mixtures. The addition level of CE1 was 0.2% for the CE1-0.2% mixture. The addition levels of CE2 were 0.2%, 0.4%, and 0.6% by mass of binder respectively for CE2-0.2%, CE2-0.4%, and CE2-0.6% mixtures.

The mixtures were prepared in a conventional planetary mixer according to the following protocol: (1) manually mixing PCE with water for 10 s; (2) adding water (and PCE) to PC and mixing the paddle at 140 rpm for 30 s; (3) adding sand and mixing the paddle at 140 rpm for 30 s; (4) mixing the paddle at 285 rpm for 30 s; (5) scraping and resting for 90 s; (6) mixing the paddle at 285 rpm for 60 s; (7) adding RDP or CE and mixing at 285 rpm for 60 s.

In addition, big mortar batches (20 liters) were prepared in a pan mixer for 3D printing experiments according to the following protocol: (1) manually mixing PCE with water for 10 s; (2) mixing dry materials (sand and PC) for 30 s; (3) adding water (and PCE) to the dry materials and mixing for 180 s; (4) scraping and resting for 60 s; (5) adding RDP or CE and mixing for 60 s.

Concrete slabs (1000 mm × 500 mm × 50 mm) were roughened by grit blasting with a pressure of 0.7 MPa to replace the tunnel wall rock. The concrete, where the slabs are composed of, contains CEM I 52.5 N (PC) (same type as mentioned before) 470 kg/m³, water 188 kg/m³, river sand (0-2 mm) 750 kg/m³, and gravel (2-8 mm) 946 kg/m³. The compressive strength and tensile strength of the slabs amounted to 35.3 MPa (150 mm cubic mold) and 3.6 MPa (50 mm drilled core) respectively after curing for 28 days

according to the standards NBN EN 12390-3 (2009) (20) and NBN EN 1542 (1999) (21), respectively. The roughness index R_q (root mean square roughness value, unit mm) of the concrete slabs was 0.33 mm which was determined by an automated laser measurement equipment (sensor ILD 1800-50, Micro-epsilon mess-tech GmbH, resolution 5 μm) (22) and calculated according to the standard BS 1134 (2010) (23). A concrete plate (diameter 50 mm) was drilled from the concrete slab for the tack test. A stroke of 1000 mm \times 200 mm \times 50 mm and seven strokes of 1000 mm \times 80 mm \times 50 mm were sawed from the slab for the upside-down printing test, which will be further described in the following sections.

2.2. Testing procedures

2.3.1 Tack test

A tack test was performed to analyze the adhesion performance of the fresh mixtures. A rheometer (MCR 102, Anton Paar) with a parallel-plate geometry (diameter 50 mm) was used. The concrete plate (diameter 50 mm) drilled from the grit-blasted concrete slab was glued to the top plate geometry. In addition, a sandpaper (diameter 50 mm, root mean square roughness value R_q 0.18 mm) was fixed to the bottom plate to avoid slippage.

The test protocol of the tack test was as follows: (1) a plastic circular mold (height 20 mm, diameter 50 mm) was placed on the bottom plate; (2) fresh mixtures were placed and

compacted in the mold and then demolded to obtain a similar initial state for each sample; (3) the grit-blasted concrete plate, which was placed in water for 24 hours, was dried with a paper towel before the tack test for a surface saturation dry condition; (4) the grit-blasted surface was treated with the fresh mixture and scraped (to obtain the same condition as during the upside-down printing test, which will be further explained in the following section); (5) the plate was moved downwards until a gap of 10 mm was obtained, which was equal to the thickness of one printed layer. In this way, full-contact between the grit-blasted concrete plate and the fresh mixture was achieved and a similar squeezing process was also observed when the material was extruded against the slab; (6) the grit-blasted concrete plate was pulled off and the normal force versus displacement curves were recorded. For each mixture, the test was repeated five times with a new mixture. The test process is shown in Fig. 2.

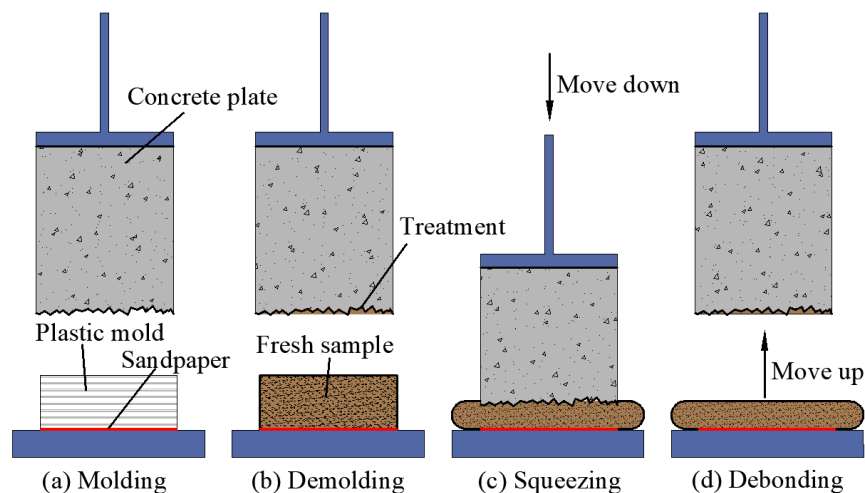


Fig. 2 Schematic view of tack test.

Normally, a tack test is performed in a displacement controlled mode where the pull-off velocity is constant during the whole test (18, 19). In this study, the test was carried out in a load control mode, where linearly increasing loads were applied by the grit-blasted concrete plate to mimic the stepwise increasing loads of the 3D printing process, as shown in Fig. 3.

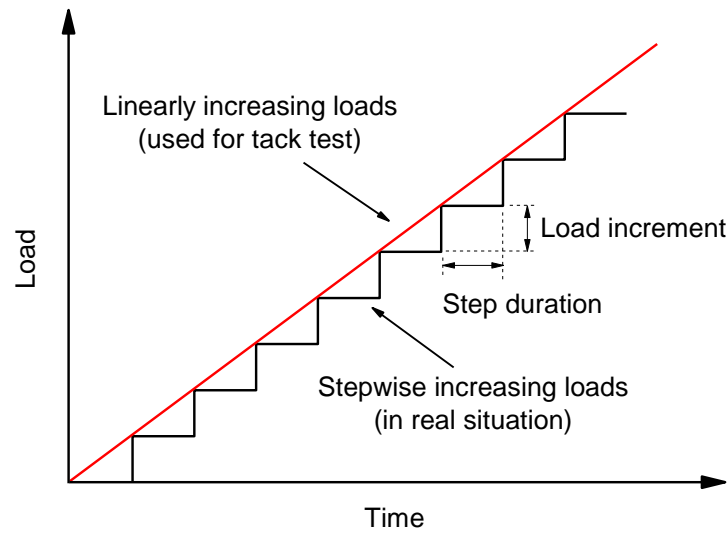


Fig. 3 Linearly increasing loads during the tack test.

The gravity-induced load increment by one printed layer is expressed as follows:

$$\Delta F = \rho \cdot g \cdot V = \rho \cdot g \cdot l \cdot \omega \cdot h \quad (1)$$

Where ρ is the density (kg/m^3), g is the gravitational constant, taken as 9.81 m/s^2 , l is the constant path length of each layer (m), ω is the layer width (m), h is the layer thickness (m). The normal stress increment $\Delta\sigma$ (Pa) can thus be expressed as follows:

$$\Delta\sigma = \frac{\Delta F}{A} = \rho \cdot g \cdot h \quad (2)$$

Where A is the area of one printed layer (m^2), which can be calculated as follows:

$$A = l \cdot \omega \quad (3)$$

The duration of one loading step is expressed as follows:

$$\Delta t = \frac{l}{v} + t_0 \quad (4)$$

Where v is the printing speed (m/s) and t_0 is the break time (s) between two layers without the extrusion of material. Therefore, the applied loading rate in the tack test is derived from the gravity-induced stress and expressed as follows:

$$\dot{F}_T = \frac{\Delta\sigma}{\Delta t} \cdot \frac{\pi d^2}{4} = \frac{\pi \rho g h d^2}{4 \left(\frac{l}{v} + t_0 \right)} \quad (5)$$

Where \dot{F}_T is the applied loading rate (N/s) in the tack test and d is the plate diameter (m). In this study, the density ρ is 2000 kg/m^3 , the layer thickness h is 0.01 m , the printing speed v is 0.1 m/s , the plate diameter is 0.05 m , the path length of each layer l is 0.6 m , and the estimated break time t_0 is 4 s . Therefore, the loading rate in the tack test is calculated as 0.04 N/s .

2.3.2 Stress growth test

A stress-controlled rotary rheometer (MCR 52, Anton Paar) was employed to perform the stress growth test. A building material cell and a 6-bladed vane rotor were used. The inside

of the building material cell was provided with 24 vertical ribs (square column, width 0.5 mm) uniformly distributed around the inner surface of the cell to prevent wall slippage. The yield stress was measured by applying a constant low rotational speed (0.2 rpm) to the material, starting from rest and lasting for a maximum period of 200 s. The test was repeated five times for each mixture. A schematic view of the building material cell and the vane rotor is shown in Fig. 4.

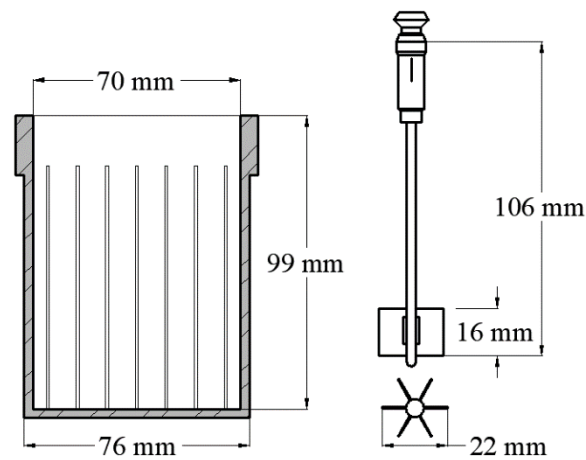


Fig. 4 Schematic view of the building material cell and vane rotor.

2.3.3 Sag resistance test

A 6-axis robotic arm (ABB IBR 6650) was used for controlling the nozzle position, and a worm pump (MMB STROBOT 407) with a pumping pipe (diameter 25.4 mm, length 3 m) was used for material extrusion. A custom-made plastic nozzle with a trowel (material:

standard PLA, printer: Ultimaker 2+) was printed for surface smoothing, as shown in Fig. 5.

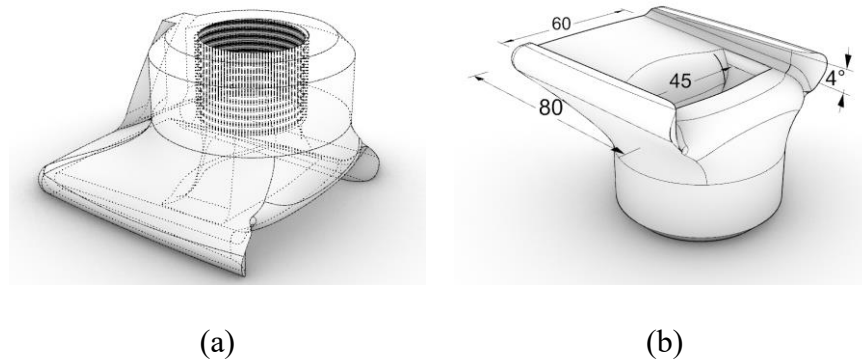


Fig. 5 Schematic view of the nozzle with trowel, (a) perspective, and (b) dimensions (mm).

The first aim was to verify the sag resistance of the mixtures and an upside-down printing experiment was performed. The stroke of 1000 mm x 200 mm x 50 mm was used to replace the overhead position of the tunnel wall rock. The strokes were soaked in water 24 hours prior to the printing experiment. Before printing, the grit-blasted surface was dried with a paper towel to obtain a saturated surface dry condition, which is considered as the optimal condition in many cases (24). After that, the surface was treated with the fresh mixture which was going to be printed and scraped to fill some gaps within the grit-blasted surface in advance, which is also a common procedure when applying repair mortars to guarantee good performance (24, 25). The slab was fixed on a steel frame (height 2 m) with its grit blasted, saturated surface dry, pretreated surface faced downwards. The printing system is shown in Fig. 6.

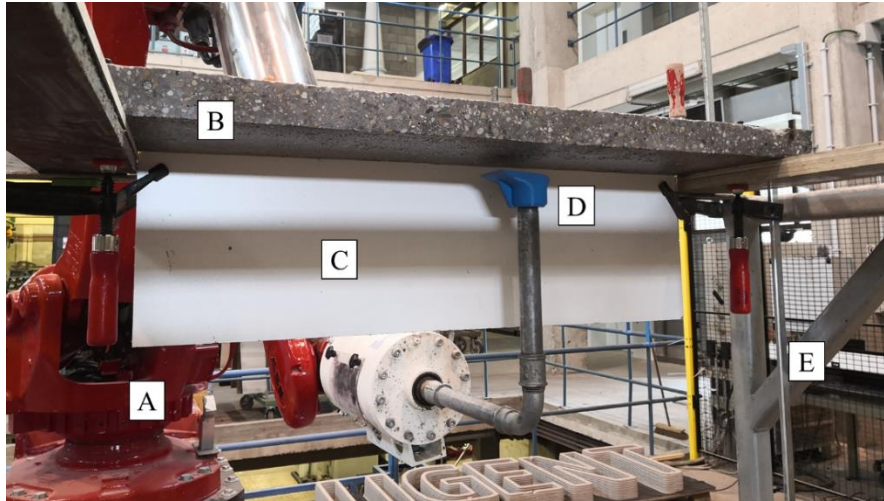


Fig. 6 3D printing system. A: 6-axis robotic arm; B: Grit blasted concrete slab; C: White background; D: Plastic nozzle; E: Steel frame.

The fresh materials were printed upside down at the lower face of the concrete stroke. The length of the subsequent layer was 4 mm shorter on the two lateral sides compared to the previous layer for avoiding boundary effects at the two lateral sides. The printing speed was set as 100 mm/s and layers with the following dimensions were printed: length (of the first layer) 600 mm, width 60 mm, and thickness 10 mm. The printing process was recorded and ended when failure occurred. After each experiment, the grit-blasted surface was washed and water at the surface was removed with a paper towel to obtain a saturated surface dry condition again for the next experiment. The test was repeated two times for each mixture. A schematic view of the upside-down printing process is illustrated in Fig. 7.

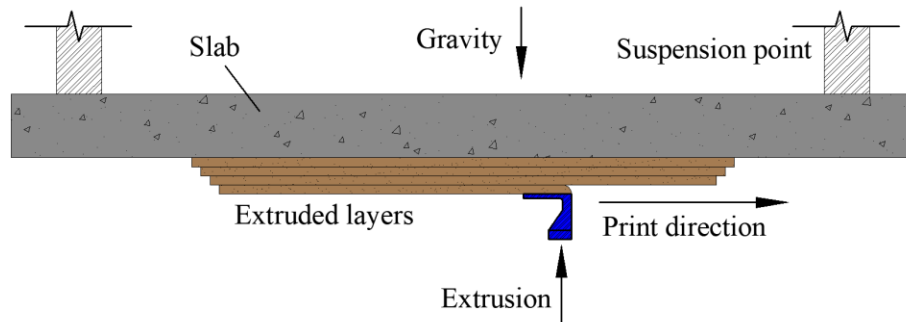


Fig. 7 Schematic view of the upside-down printing.

2.3.4 Pull-off test

The second aim was to evaluate the bond strength of the mixtures in the hardened stage. From the previously mentioned concrete slabs (see section 2.1) seven strokes of 1000 mm × 80 mm × 50 mm were cut and soaked in water 24 hours prior to the print experiment. The grit blasted surface was dried with a paper towel and treated with the fresh material in the same way as described in section 2.3.3 before the experiment. A three-layered element (length 600 mm, width 60 mm, total thickness 30 mm) was printed with a movement speed of 100 mm/s at the lower face of the concrete slab for each mixture.

The samples were kept in the testing hall for one day and cured in a controlled environment (temperature 20 °C, relative humidity 65%) for 6 more days, the printed element was drilled to a depth of 15 mm into the concrete substrate with a core drill (diameter 50 mm) and then a dolly was glued to the core face. The pull-off test was performed with an automatic bond strength device (Proceq DY-2, maximum tensile force 16 kN, loading rate

0.05 MPa/s, calibrated accuracy 1%) according to EN 1542 (21). The maximum force required to pull-off the core was measured (26). The test was performed three times for each series. A schematic view of the pull-off test is shown in Fig. 8.

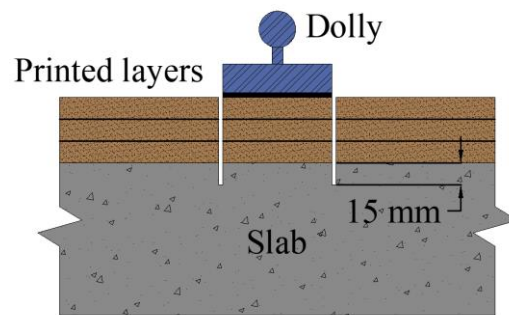


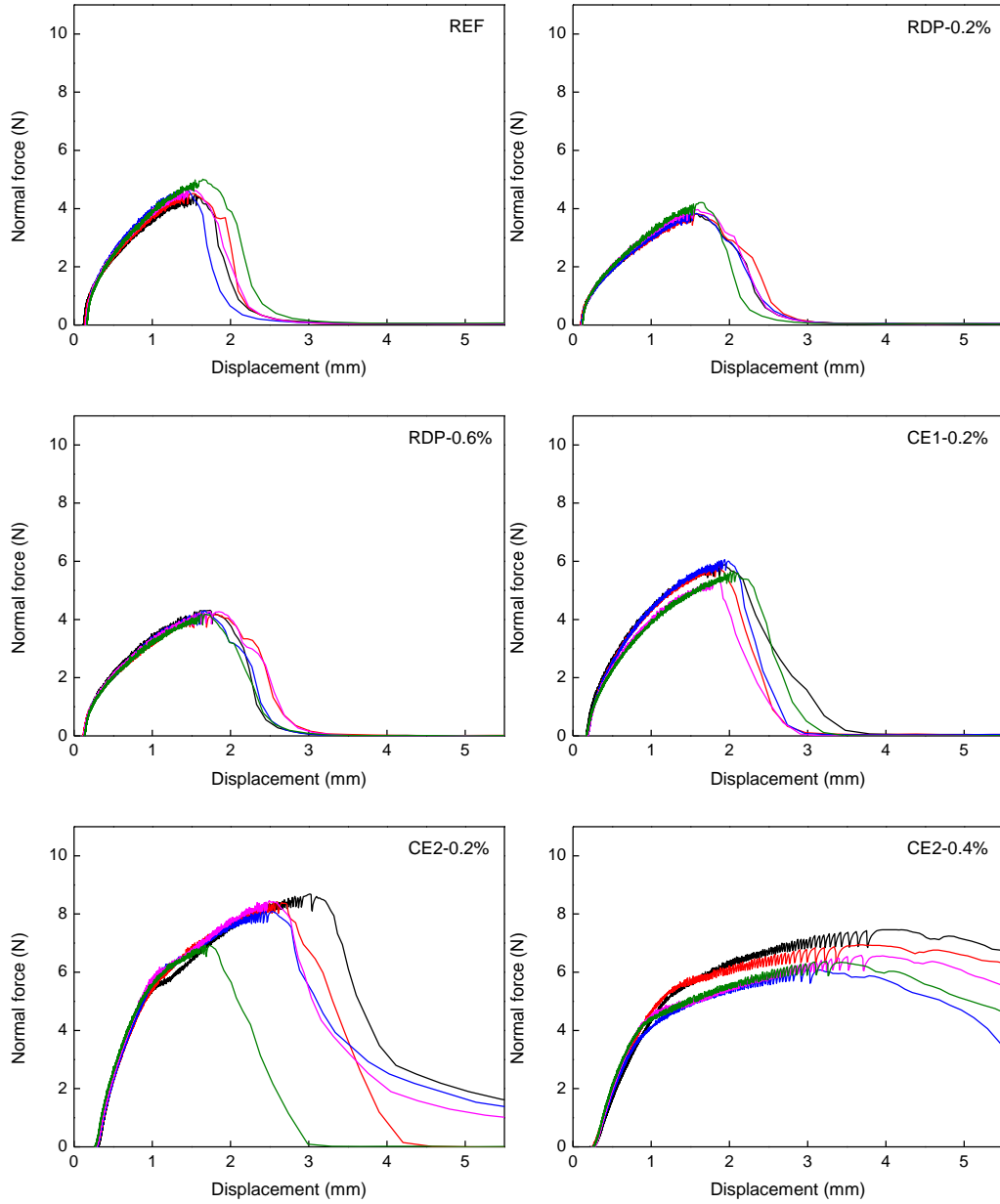
Fig. 8 Schematic view of pull-off test.

3. Results and discussion

3.1. Normal force versus displacement curves

Normal force versus displacement curves were obtained from the tack test, as shown in Fig. 9. The curves showed that the tested samples followed two main stages. In the first stage, the normal force increased from zero to a peak value, where an inward flow with a small displacement was observed. The second stage was characterized by a debonding behavior where the normal force dropped sharply from the peak value to zero and the displacement suddenly increased to a maximum value. It should be noted that CE-modified

mixtures, especially for CE2 presented quite long increase stages, which will be explained in the following sections.



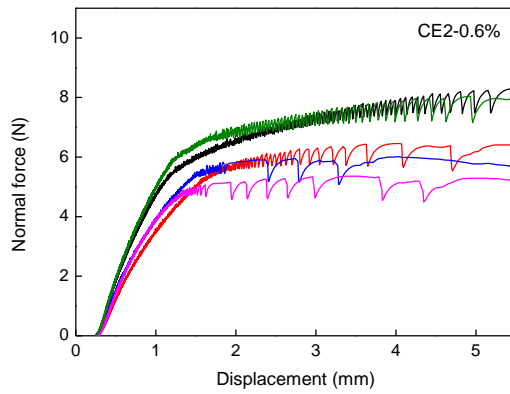


Fig. 9 Normal force versus displacement curves.

The first issue to be discussed relates to the source of the tack effort which has to be exerted to separate the two surfaces, as well as the failure mode. The failure mode of the fresh sample in the tack test after debonding was recorded, as shown in Fig. 10.

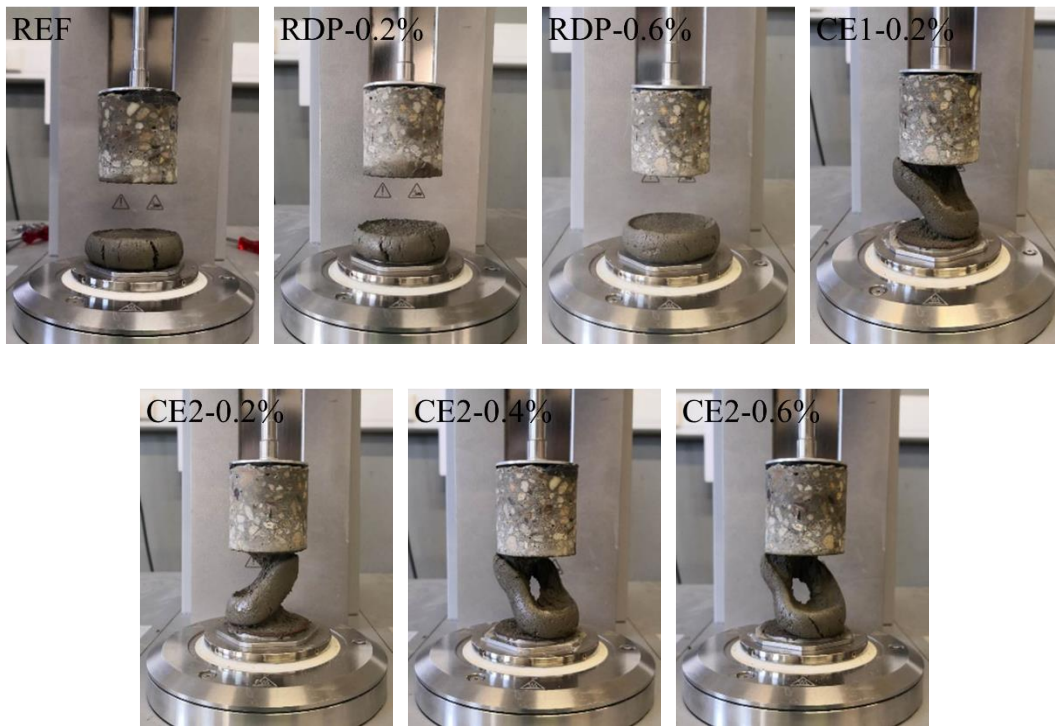


Fig. 10 Failure mode in the tack test.

It was shown that the adhesive failure (i.e. failure occurring at the interface between the fresh sample and the concrete slab) occurred when we tested the reference mixture (REF) and the two RDP-modified mixtures (i.e. RDP-0.2% and RDP-0.6%). While cohesive failure (i.e. failure occurring inside the fresh material) occurred when we tested the four CE-modified mixtures (i.e. CE1-0.2%, CE2-0.2%, CE2-0.4%, and CE2-0.6%). In previous studies, Mohamed Abdelhaye et al. (16) presented the tackiness of mud and pointed that the physical origin of the effort required to separate the plates could be the force required to overcome the Laplace depression (or capillary pressure) in the mud layer, generated by the curvature of the meniscus at the mud-plate interface as the mud layer was put in tension (27). In addition, another physical explanation was that the effort required to lift the plates was the force required to force the inwards flow of the mud and the flow was almost entirely radial shear flow in the early stages of the lifting process (15). A small increase in plate separation induced a large inward motion of the mud, which was the same phenomenon as was observed during the tack test of the mixtures formulated in this study. In addition, Mohamed Abdelhaye et al. (16) also pointed that the failure associated with the effort required to separate the plates was either cohesive rupture in the mud layer or adhesive fracture at the mud-solid interface. Four types of failure profiles of mortars (i.e. cohesive rupture, adhesive rupture, liquid behavior, and mortar behavior) were described by Kaci et al. (28) while the failure mode of paste was always found to be cohesive, that is, occurring within the layer of paste, whatever the type of paste and the type of de-

bonding experiment (29). In this study, the failure occurred at the interface between the grit-blasted concrete plate and fresh sample for the reference mixture and the RDP-modified mixtures, rather than inside the fresh mortar mixtures, indicating that the interface was a weak spot of the mixtures in the fresh stage. This result can be interpreted in terms of the presence of sand in the fresh sample which increased the overall shear stress and contributed a lot to the shear resistance (30). It was pointed out that shear stress in mortar is more complicated than shear stresses in pastes or muds. The overall shear stress of a flowing mortar can be taken as the sum of the shear stress resulting from the yield stress of the cement paste, the flow of the cement paste, the interaction between cement paste and aggregates, and the shear stress resulting from the aggregate movement (30). Thus the aggregate content seems to have a significant effect on the inward flow of tested samples, the failure mode (e.g. adhesive failure or cohesive failure), and the force required for debonding. Therefore, it can be concluded that the flow resistance of the sample towards the center of the plates dominated the increasing stage (e.g. the evolution of deformation towards the critical displacement where the peak normal force occurred). The peak normal force was determined by the adhesion properties at the interlayer position when adhesive failure occurred, while the peak normal force was determined by the shear resistance of the fresh material when cohesive failure occurred. The reason why CE-modified mixtures presented a different normal force versus displacement profile was that a high dosage of CE admixture enhanced the adhesion at the interface while it decreased the shear resistance, which will be further explained below.

To go one step further, the peak normal force is shown in Fig. 11. A one-way ANOVA test was used to statistically analyze the influence of the addition of RDP or CE on the peak normal force obtained in the tack test. A p value less than 0.05 ($p < 0.05$) was considered statistically significant. According to the one-way ANOVA test, the RDP-modified mixtures had no significant different peak normal force compared to the reference mixture (REF) while all CE-modified mixtures presented a significant difference. It was also shown that the peak normal force was slightly decreased with the addition of RDP, compared to the reference mixture (REF). While all the CE-modified mixtures showed a higher peak normal force compared to the reference mixture (REF). In addition, the CE2-0.2% mixture showed a higher peak normal force than the CE1-0.2% mixture. For CE2-based mixtures, the increase in CE2 admixture addition level (i.e. 0.4% and 0.6%) did not result in a further enhancement of the peak normal force compared to the CE2-0.2% mixture, indicating that the adhesion enhancement of the CE2 admixture was limited.

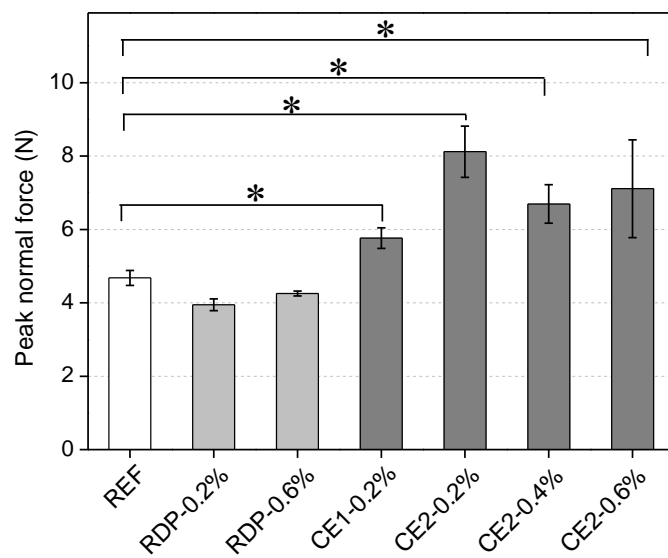


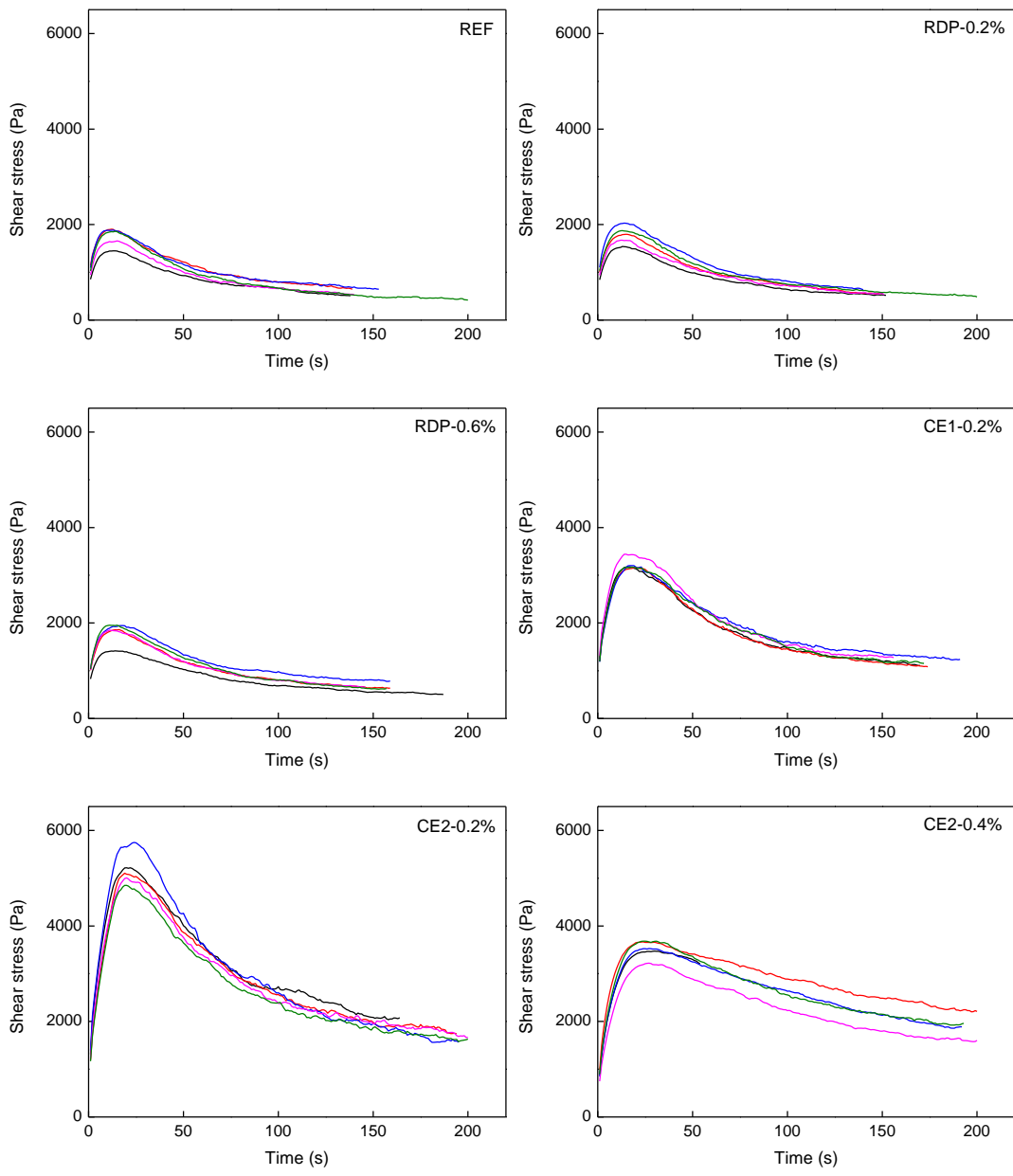
Fig. 11 Peak normal force of the mixtures (error bar represents the standard deviation, symbol “*” indicates a significant difference with a level of $p < 0.05$).

In previous studies, RDP has been demonstrated to improve the bond strength in hardened state to various substrates (9). Normally, it would take a long time for polymer particles to flocculate and form polymer films with the drainage of water between polymer particles (8). However, the testing period of a tack test (normally less than 10 minutes) was too short to allow the formation of polymer films.

That CE enhanced the peak normal force can be explained by the absorption effect. After coming into contact with the grit-blasted concrete plate, CE can absorb on the concrete surface either by hydrogen bonding or by specific interaction involving the hydroxyl groups of CE and the concrete surface, resulting in a better adhesion performance (7). Compared to CE1 (viscosity 400-700 mPa·s), CE2 (viscosity 28000-34000 mPa·s) possessed more functional groups and therefore resulted in a higher peak normal force. In addition.

3.2. Flow resistance

The shear stress versus time curves are shown in Fig. 12. It was shown that the shear stress increased after the measurement started, followed by a decreasing stage. The peak shear stress was treated as the yield stress.



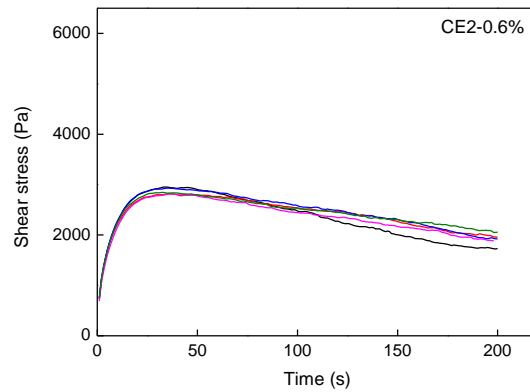


Fig. 12 Shear stress versus time curves.

To better understand the results, the yield stresses of the mixtures are shown in Fig. 13. A one-way ANOVA test was used to statistically analyze the influence of the addition of RDP or CE on the yield stress obtained in the stress growth test. A p value less than 0.05 ($p < 0.05$) was considered statistically significant. According to the one-way ANOVA test, the RDP-modified mixtures had no significant different yield stress compared to the reference mixture (REF) while all CE-modified mixtures presented a significant difference. The results showed that the mean yield stresses of the two RDP-modified mixtures (RDP-0.2% and RDP-0.6%) were 1781.81 Pa and 1806.36 Pa respectively, being almost the same as the mean value obtained for the reference mixture (1750.05 Pa). On the contrary, the yield stress of the four CE-modified mixtures (CE1-0.2%, CE2-0.2%, CE2-0.4%, and CE2-0.6%) was distinctly higher than the value obtained for the reference mixture. In addition, the increase in yield stress became less pronounced when the dosage of CE2 increased from 0.2% to 0.6%. The CE2-0.2% mixture possessed a maximum mean yield stress value of 5185.61 Pa.

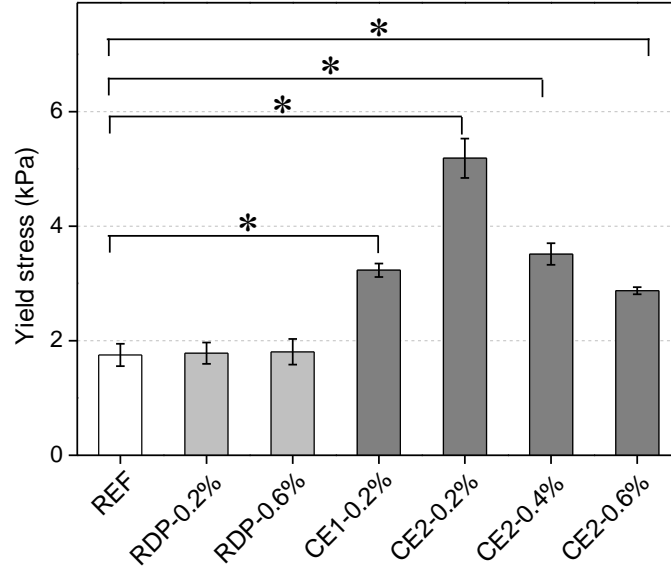


Fig. 13 Yield stress of the mixtures (error bar represents the standard deviation, symbol “*” indicates a significant difference with a level of $p < 0.05$).

Previous studies pointed out that RDP decreased the yield stress because of the ball bearing action of polymer particles, the entrained air, and the dispersing effect of surfactants in RDP products (31). Ohama et al. studied the influence of polymer-cement ratio on the fluidity by the slump test and showed that the water-cement ratio at a given slump is markedly reduced with an increase in the polymer-cement ratio (9). It was also pointed out that RDP had a relatively small dimension compared to that of cement particles (9) and therefore worked as a lubricant in the fresh cement-based materials, leading to smaller yield stress and higher workability. While in this study, there is no significant difference between the reference mixture and RDP-modified mixtures, which can be explained by the relatively low addition level (0.2% and 0.6%).

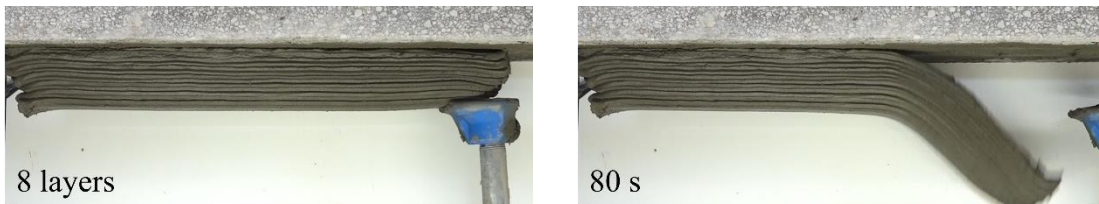
The function of CE in changing yield stress can be explained by a combination of different physicochemical phenomena that depend on the nature of the CE and its concentration (32). An increase of the yield stress involved a bridging flocculation mechanism, where the chain of CE would be adsorbed onto two or more cement particles, physically holding them together (33). Therefore, with more functional groups, mixture CE2-0.2% obtained a much higher mean yield stress (5185.61 Pa) than mixture CE1-0.2% (3230.48 Pa).

Regarding the impact of CE dosages on the yield stress, contradictory results have been found in literature. Some authors held the opinion that a high dosage of CE would increase the yield stress because of depletion flocculation where non-absorbed polymers were depleted from a volume exclusion shell around large particles. The difference in polymer concentration in bulk solution with respect to the depleted zone led to an increase of the osmotic pressure in the system, which caused the flocculation. (11). Some authors confirmed that CE would decrease the yield stress (34). Jenni et al. investigated the role of CE on changes in mortar microstructures (10). They proposed that the air entrapped during the mixing process was stabilized in the fresh mixture due to the decrease of the surface tension of water and the accumulation of CE at the air-void interfaces. It was also pointed by Wyrzykowski et al. (35) that a coarsening of the porosity and a slight increase in the total volume of pores occurs at a higher dosage of CE. This is likely due to the agglomeration of original subspherical pores, found to be more pronounced for the increased CE dosage. Therefore, the yield stress decreased due to the increased proportion of air content inside the fresh mixture where air acted as a lubricant (36). Another

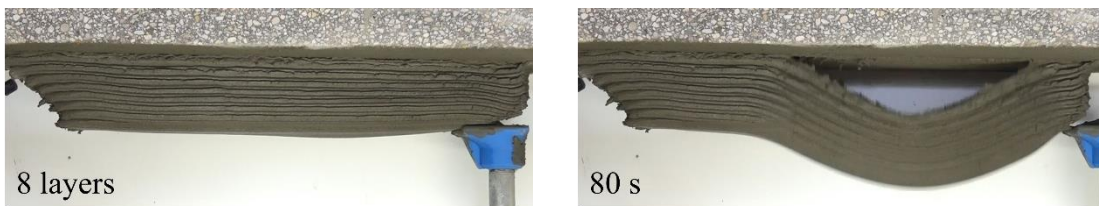
explanation of this decrease was the steric hindrance induced by the CE adsorbed onto cement particles (37).

3.3. Upside down printing

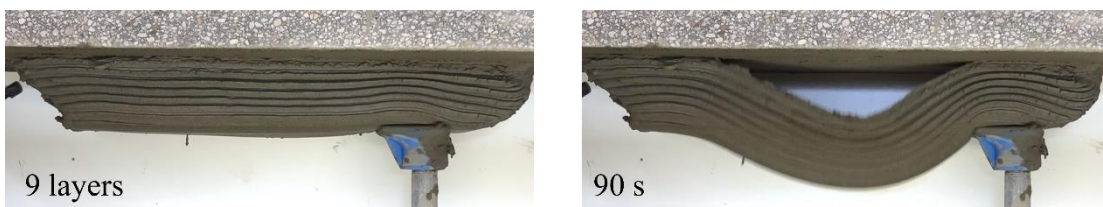
A 3D concrete printing test, involving printing upside down against the lower face of a supported concrete slab, was performed. The tests were repeated two times for each mixture and only one of both experiments is shown in Fig. 14.



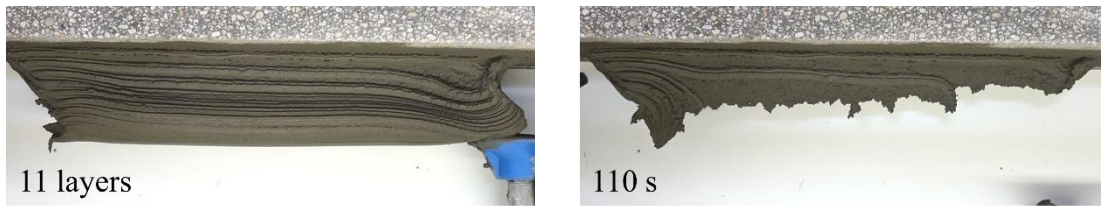
(a) REF



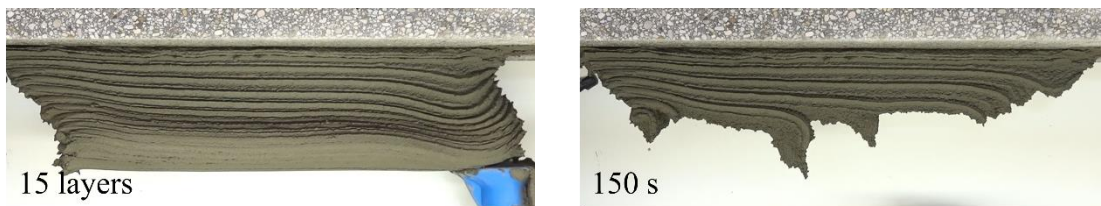
(b) RDP-0.2%



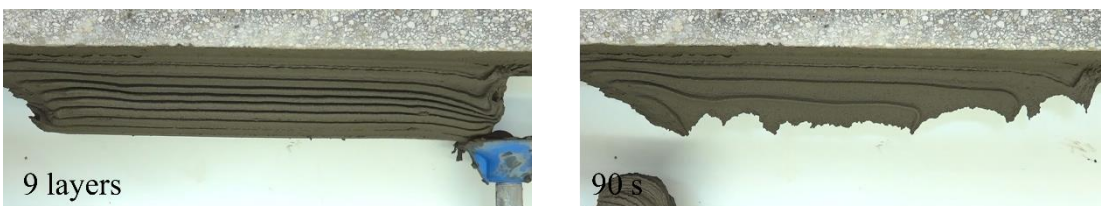
(c) RDP-0.6%



(d) CE1-0.2%



(e) CE2-0.2%



(f) CE2-0.4%



(g) CE2-0.6%

Fig. 14 Upside printing test: left figures represent maximum amount of layers and right figures represent failure modes.

More details can be found in Table 1. Failure mode “adhesion” represents that failure occurred at the interface between the fresh material and the concrete slab, while failure mode “cohesion” represents that failure occurred at the interlayer position inside the fresh material.

Table 1 Maximum amount of layers and failure mode (including adhesive failure and cohesive failure).

No.	Mixture	Maximum layers	Failure mode
1	REF	8 8	Adhesion
2	RDP-0.2%	8 9	Adhesion
3	RDP-0.6%	9 10	Adhesion
4	CE1-0.2%	9 11	Adhesion Cohesion
5	CE2-0.2%	12 15	Cohesion
6	CE2-0.4%	9 10	Cohesion
7	CE2-0.6%	8 8	Cohesion

The reference mixture (REF) and the two RDP-modified mixtures (RDP-0.2% and RDP-0.6%) showed adhesive failure, indicating an insufficient adhesive strength. One CE-modified mixture (CE1-0.2%) presented either adhesive failure or cohesive failure. The other three CE-modified mixtures (CE2-0.2%, CE2-0.4%, and CE2-0.6%) only presented cohesive failure, indicating a strong adhesion at the position of the interface but relatively low shear resistance (i.e. low yield stress). The results of the upside-down printing tests

are in accordance with the tack test results, which were shown in **Error! Reference source not found.**

Assuming that failure occurs at the interface, the peak normal force obtained from the tack test can be used to predict the maximum amount of layers (i.e. construction thickness). The maximum amount of layers can be calculated as follows:

$$n = \frac{F_{max}}{\rho g h \cdot \frac{\pi d^2}{4}} \quad (6)$$

Where F_{max} is the peak normal force (N) measured in the tack test. The density ρ is 2000 kg/m³, g is the gravitational constant, taken as 9.81 m/s², the layer thickness h is 0.01 m, the plate diameter d is 0.05 m.

On the other hand, assuming that failure occurs inside the fresh material, the yield stress obtained from the stress growth test can be used to predict the maximum number of layers. The maximum number of layers can be calculated as follows, giving that $\sigma_0 = \sqrt{3}\tau_0$ for a von Mises solid (38):

$$n = \frac{\sigma_0}{\rho g h} = \frac{\sqrt{3}\tau_0}{\rho g h} \quad (7)$$

Where σ_0 is the normal stress (Pa) and τ_0 is yield shear stress (Pa).

The maximum amount of layers for all mixtures predicted by the tack test, the stress growth test, and obtained from the upside-down printing test are shown in Fig. 15.

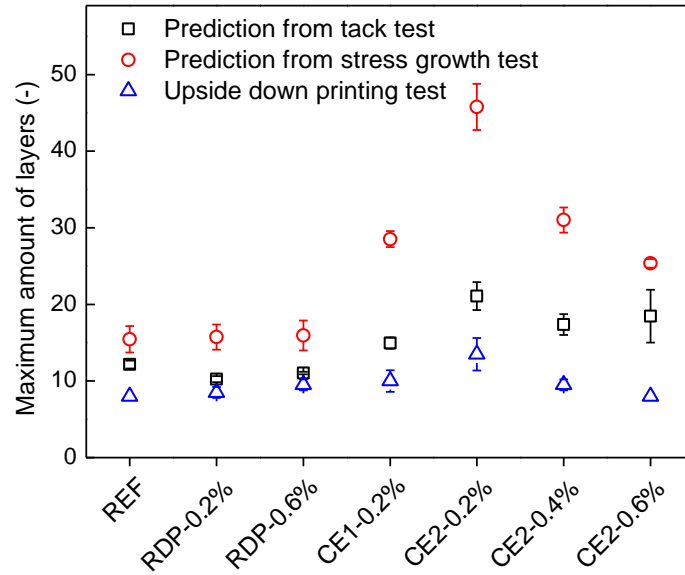


Fig. 15 Comparison among the tack test, the stress growth test, and the 3D printing test (symbols represent individual values, error bars represent standard deviation).

The results showed that the prediction from the tack test and the prediction from the stress growth test were qualitatively consistent with the results of the upside-down printing test. It should be noted that with the increase in CE2 dosage from 0% (REF mixture) to 0.2%, the maximum number of layers predicted from the tack test increased from 12 layers to 21 layers, indicating an enhanced adhesion performance, as also confirmed by the upside-down printing test (from 8 layers to an average value of 13.5 layers). Furthermore, with the increase of CE2 dosage from 0.2% to 0.6%, the predicted number of layers from the tack test reached a plateau while the prediction from the stress growth test decreased from 21 layers to 18 layers, indicating that poor shear resistance played the key role, as also confirmed by the upside-down printing test, where failure occurred inside the printed material and the maximum number of layers decreased from 13.5 (average value) to 8.

In addition, we observed that the tack test results were quantitatively closer to the outcome of the printing test, compared to that of the stress growth test. This can be interpreted by the envelop curve of Mohr criteria, as shown in Fig. 16. In the figure, A represents the material without any normal stress, which can be reflected by yield stress measured by the stress growth test. B represents the material in a tension state, which was related to either the tack test or the upside-down printing situation. C represents the material under compression, which is related to traditional 3D concrete printing situations. Without the consideration of normal stress, the predicted value provided by the stress growth test was higher than that provided by the tack test, which was also in good agreement with the obtained results (see Fig. 15).

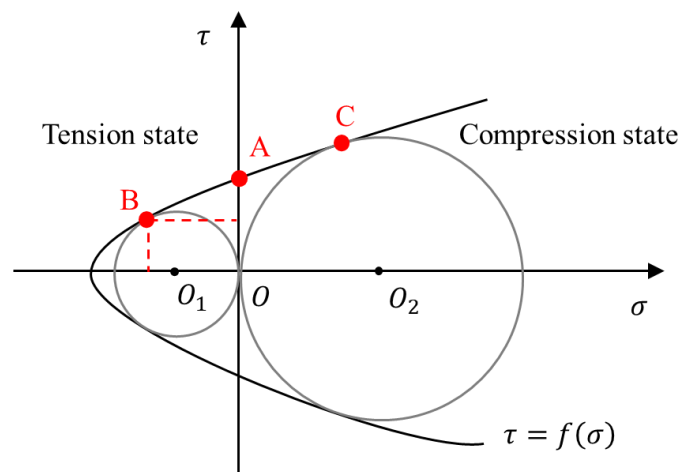


Fig. 16 Envelop curve of Mohr criteria.

3.4. Bond strength

The bond strength of the mixtures after curing for 7 days was measured, as shown in Fig. 17.

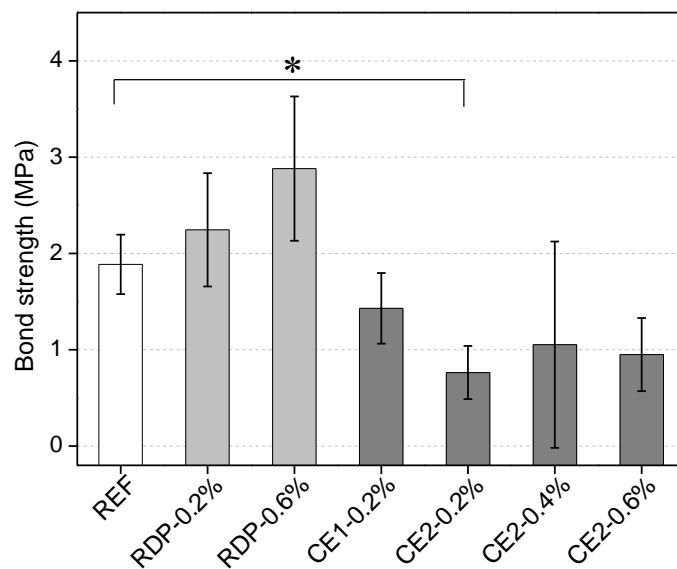


Fig. 17 Bond strength after curing for 7 days (error bar represents the standard deviation, symbol “*” indicates a significant difference with a level of $p < 0.05$).

A one-way ANOVA test was used to statistically analyze the influence of the addition of RDP or CE on the bond strength obtained in the pull-off test. A p value less than 0.05 ($p < 0.05$) was considered statistically significant. According to the one-way ANOVA test, the bond strength of the CE2-0.2% mixture presented a significant difference compared to that of the reference mixture (REF). Nevertheless, it was also shown that RDP enhanced the mean value of the bond strength while CE harmed the mean value of the bond strength.

The improvement of RDP on the bond strength is discussed firstly. In this study, the RDP addition level was much lower than in other commonly adopted RDP-modified mixtures (17). Still, the mean bond strength of the RDP-0.6% mixture (2.88 MPa) was increased by 52.38% compared to that of the REF mixture (1.89 MPa). It was pointed out that the RDP modification of cement mortar and concrete was governed by both cement hydration and polymer film formation processes in their binder phase. When RDP was mixed with fresh cement mortar, the polymer particles were uniformly dispersed in the cement paste phase. With drainage due to the development of the cement gel structure, the polymer particles were gradually confined (10) and the films or membranes bound the RDP-modified mixtures and the grit-blasted concrete slab to form an additional connection. Previous studies presented a nearly ten-fold increase in bond strength of RDP-modified mortar with a polymer-cement ratio of 20%, compared to unmodified mortar (9).

Palacios and Flatt (11) pointed out that CE is highly hydrophilic and has a high capacity to bind water molecules, increasing their effective volume in solution. This function led to an increase in the dynamic viscosity of the interstitial solution. Therefore, a high dosage of CE would prevent water to move into the porous substrate and corresponding iron migration at the position of the interface, leading to an impaired bond strength.

4. Conclusions

The effect of redispersible polymer powder (RDP) and cellulose ether (CE) on the sag resistance and bond strength of printable concrete for rock tunnel linings was studied. A

tack test, a stress growth test, an upside-down printing test, and a pull-off test were performed. According to the results and the discussion, the following conclusions can be drawn:

- (1) The sag resistance of printable concrete was related to two aspects including the adhesion at the interface and the shear resistance of the fresh material itself. The adhesion and shear resistance properties determined two different failure modes including the adhesion failure (i.e. failure occurred at the interface) and cohesion failure (i.e. failure occurred in the fresh material).
- (2) RDP presented no significant effect on the sag resistance, while CE enhanced adhesion at the interface because of its absorption onto the grit-blasted concrete surface. However, a high addition level of CE did impair the shear resistance because of air entrainment, resulting in a transition from an adhesive failure to a cohesive failure.
- (3) The maximum number of printed layers and failure modes in the upside-down printing test was more qualitatively predicted by the tack test, compared to the stress growth test. This is because the fresh material in the tack test and the printing test followed a similar tension state.
- (4) RDP increased the bond strength of printable concrete in the hardened stage with film formation. The bond strength of CE-modified mixtures was lower than that of the reference mixture because the water was trapped by CE in the fresh concrete, leading to a dehydrated interface structure.

References

1. Salvador RP, Cavalaro SH, Segura I, Figueiredo AD, Pérez J, "Early age hydration of cement pastes with alkaline and alkali-free accelerators for sprayed concrete," *Constr Build Mater*, V. 111. 2016, pp. 386-98.
2. Galan I, Baldermann A, Kusterle W, Dietzel M, Mittermayr F, "Durability of shotcrete for underground support– Review and update," *Constr Build Mater*, V. 202, 2019/03/30/. 2019, pp. 465-93.
3. Soldo L, Vendramini M, Eusebio A, "Tunnels design and geological studies," *Tunnelling and Underground Space Technology*, V. 84, 2019/02/01/. 2019, pp. 82-98.
4. Pfeuffer M, Kusterle W, "Rheology and rebound behaviour of dry-mix shotcrete," *Cem Concr Res*, V. 31, No. 11. 2001, pp. 1619-25.
5. Khoshnevis B, "Automated construction by contour crafting—related robotics and information technologies," *Automat Constr*, V. 13, No. 1. 2004, pp. 5-19.
6. De Schutter G, Lesage K, Mechtcherine V, Nerella VN, Habert G, Agusti-Juan I, "Vision of 3D printing with concrete — Technical, economic and environmental potentials," *Cem Concr Res*, V. 112, 2018/10/01/. 2018, pp. 25-36.
7. Brumaud C, Bessaies-Bey H, Mohler C, Baumann R, Schmitz M, Radler M, et al., "Cellulose ethers and water retention," *Cement Concrete Research*, V. 53. 2013, pp. 176-84.
8. Assaad JJ, "Development and use of polymer-modified cement for adhesive and repair applications," *Constr Build Mater*, V. 163, 2018/02/28/. 2018, pp. 139-48.
9. Ohama Y, "Handbook of polymer-modified concrete and mortars: properties and process technology." William Andrew; 1995.
10. Jenni A, Holzer L, Zurbriggen R, Herwegh M, "Influence of polymers on microstructure and adhesive strength of cementitious tile adhesive mortars," *Cem Concr Res*, V. 35, No. 1. 2005, pp. 35-50.
11. Aïtcin P-C, Flatt RJ, "Science and technology of concrete admixtures." Woodhead publishing; 2015.
12. Petit J-Y, Wirquin E, "Evaluation of various cellulose ethers performance in ceramic tile adhesive mortars," *International Journal of Adhesion and Adhesives*, V. 40, 2013/01/01/. 2013, pp. 202-9.
13. Pourchez J, Ruot B, Debayle J, Pourchez E, Grosseau P, "Some aspects of cellulose ethers influence on water transport and porous structure of cement-based materials," *Cement Concrete Research*, V. 40, No. 2. 2010, pp. 242-52.
14. Lakrouit H, Sergot P, Creton C, "Direct observation of cavitation and fibrillation in a probe tack experiment on model acrylic pressure-sensitive-adhesives," *The Journal of Adhesion*, V. 69, No. 3-4. 1999, pp. 307-59.
15. Derks D, Lindner A, Creton C, Bonn D, "Cohesive failure of thin layers of soft model adhesives under tension," *Journal of applied physics*, V. 93, No. 3. 2003, pp. 1557-66.

16. Mohamed Abdelhaye YO, Chaouche M, Van Damme H, "The tackiness of smectite muds. 1. The dilute regime," *Applied Clay Science*, V. 42, No. 1, 2008/12/01/. 2008, pp. 163-7.
17. Phan V-T, "Relationship between the adhesive properties and the rheological behavior of fresh mortars," *Book Relationship between the adhesive properties and the rheological behavior of fresh mortars*, Editor, ed.^eds., École normale supérieure de Cachan-ENS Cachan, City, 2012, pp.
18. Kaci A, Bouras R, Phan VT, Andréani PA, Chaouche M, Brossas H, "Adhesive and rheological properties of fresh fibre-reinforced mortars," *Cem Concr Comps*, V. 33, No. 2, 2011/02/01/. 2011, pp. 218-24.
19. Kawashima S, Chaouche M, Corr DJ, Shah SP, "Influence of purified attapulgite clays on the adhesive properties of cement pastes as measured by the tack test," *Cem Concr Comps*, V. 48, 2014/04/01/. 2014, pp. 35-41.
20. "NEN-EN 12390-3, Testing hardened concrete — Part 3: Compressive strength of test specimens." 2019.
21. "NBN EN 1542, Products and systems for the protection and repair of concrete structures - Test methods - Measurement of bond strength by pull-off," *Book NBN EN 1542, Products and systems for the protection and repair of concrete structures - Test methods - Measurement of bond strength by pull-off*, Editor, ed.^eds., City, 1999, pp.
22. De Belie N, Monteny J, Beeldens A, Vincke E, Van Gemert D, Verstraete W, "Experimental research and prediction of the effect of chemical and biogenic sulfuric acid on different types of commercially produced concrete sewer pipes," *Cem Concr Res*, V. 34, No. 12, 2004/12/01/. 2004, pp. 2223-36.
23. "BS 1134, Assessment of surface texture. Guidance and general information," *Book BS 1134, Assessment of surface texture. Guidance and general information*, Editor, ed.^eds., City, 2010, pp.
24. Bissonnette B, Courard L, Garbacz A, "Concrete surface engineering." CRC Press; 2015.
25. Sánchez M, Faria P, Ferrara L, Horszczaruk E, Jonkers HM, Kwiecień A, et al., "External treatments for the preventive repair of existing constructions: A review," *Constr Build Mater*, V. 193, 2018/12/30/. 2018, pp. 435-52.
26. Bissonnette B, Courard L, Fowler DW, Granju J-L, "Bonded Cement-based Material Overlays for the Repair, the Lining or the Strengthening of Slabs or Pavements: State-of-the-art Report of the RILEM Technical Committee 193-RLS." Springer Science & Business Media; 2011.
27. Shull KR, Flanigan CM, Crosby A, "Fingering instabilities of confined elastic layers in tension," *Physical review letters*, V. 84, No. 14. 2000, pp. 3057.
28. Kaci A, Bouras R, Chaouche M, ani P, Brossas H, "Adhesive and rheological properties of mortar joints," *Applied rheology*, V. 19, No. 5. 2009, pp. 51970.
29. Mohamed Abdelhaye YO, Chaouche M, Chapuis J, Charlaix E, Hinch J, Roux S, et al., "Tackiness and cohesive failure of granular pastes: Mechanistic aspects," *The European Physical Journal E*, V. 35, No. 6, 2012/06/14. 2012, pp. 45.

30. Lu G, Wang K, Rudolphi TJ, "Modeling rheological behavior of highly flowable mortar using concepts of particle and fluid mechanics," *Cem Concr Comps*, V. 30, No. 1, 2008/01/01/. 2008, pp. 1-12.
31. Wang M, Wang R, Yao H, Farhan S, Zheng S, Wang Z, et al., "Research on the mechanism of polymer latex modified cement," *Constr Build Mater*, V. 111, 2016/05/15/. 2016, pp. 710-8.
32. Roussel N, "Understanding the rheology of concrete." Elsevier; 2011.
33. Fellows CM, Doherty WO, "Insights into bridging flocculation," *Book Insights into bridging flocculation*, 231, Editor, ed.^eds., Wiley Online Library, City, 2005, pp. 1-10.
34. Patural L, Marchal P, Govin A, Grosseau P, Ruot B, Devès O, "Cellulose ethers influence on water retention and consistency in cement-based mortars," *Cem Concr Res*, V. 41, No. 1, 2011/01/01/. 2011, pp. 46-55.
35. Wyrzykowski M, Kiesewetter R, Münch B, Baumann R, Lura P, "Pore structure of mortars with cellulose ether additions – Study of the air-void structure," *Cem Concr Comps*, V. 62, 2015/09/01/. 2015, pp. 117-24.
36. Jiao D, Shi C, Yuan Q, An X, Liu Y, Li H, "Effect of constituents on rheological properties of fresh concrete-A review," *Cem Concr Comps*, V. 83, 2017/10/01/. 2017, pp. 146-59.
37. Patural L, Korb J-P, Govin A, Grosseau P, Ruot B, Devès O, "Nuclear magnetic relaxation dispersion investigations of water retention mechanism by cellulose ethers in mortars," *Cem Concr Res*, V. 42, No. 10, 2012/10/01/. 2012, pp. 1371-8.
38. Meeten GH, "Yield stress of structured fluids measured by squeeze flow," *Rheologica acta*, V. 39, No. 4. 2000, pp. 399-408.